Int. J. Heat Mass Transfer. Vol. 20, pp. 371–381. Pergamon Press 1977. Printed in Great Britain

DIRECT CONTACT CONDENSATION OF STEAM BUBBLES IN WATER AT HIGH PRESSURE

G. G. BRUCKER and E. M. SPARROW
Department of Mechanical Engineering, University of Minnesota, Minneapolis, Minnesota, U.S.A.

(*Received* 9 *June* 1976 *and in revised form* 22 *July* 1976)

Abstract—Experiments have been carried out to investigate direct contact condensation of saturated steam bubbles introduced into a quiescent subcooled water environment. The experiments were performed for a range of pressures from 10.3 to 62.1 bar (150–900 lb/in^2), for subcooling from 15 to 100°C, and for initial bubble diameters of about 3 mm. The data reduction of high speed motion pictures was based on a frame by frame analysis wherein the coordinates of the bubble perimeter were recorded in digital form and subsequently processed to yield quantitative information about the bubble collapse history and heat-transfer coefficient. The photographs showed that the successive shapes of the bubbles during their collapse histories proceeded from a sphere to a hemisphere to an ellipsoid to a sphere to collapse; short-lived bubbles collapsed as ellipsoids. The time to collapse and the height to collapse increased with increasing pressure and with decreasing temperature difference. The rise velocities of the bubbles were essentially constant, with an overall range of 15–22 cm/s. The average heat-transfer coefficients were on the order of 10^4 W/m$^2\cdot$°C (1750 Btu/h$\cdot$ft$^2\cdot$°F), with only modest variations with pressure level and temperature difference. The instantaneous heat-transfer coefficients did not differ appreciably from the average coefficients.

NOMENCLATURE

- A, surface area of bubble;
- A_i, initial surface area;
- c_p, specific heat at constant pressure;
- d_i, initial bubble diameter, equation (3);
- Fo_m, Fourier number based on r_{max}, $\alpha_f t/r_{max}^2$;
- Fo^*, Fourier number at collapse, $\alpha_f t^*/r_i^2$;
- g, acceleration of gravity;
- H, instantaneous height of bubble above orifice plate;
- H^*, height at collapse;
- h, instantaneous heat-transfer coefficient, equation (5);
- h^*, average heat-transfer coefficient, equation (4);
- h_{fg}, latent heat of condensation;
- Ja, Jakob number, equation (6);
- k, thermal conductivity;
- Pe, Peclet number, $RePr$;
- Pr, Prandtl number, $(c_p\mu/k)_f$;
- Ra, Rayleigh number, equation (6);
- Re, Reynolds number, $\rho_f v d_i/\mu_f$;
- r_i, initial bubble radius, equation (3);
- r_{max}, maximum bubble radius, $(3V_{max}/4\pi)^{1/3}$;
- T_{sat}, saturation temperature;
- T_∞, water temperature;
- t, time;
- t^*, time at collapse;
- V, bubble volume;
- V_i, initial bubble volume;
- V_{max}, maximum bubble volume;
- v, bubble velocity.

Greek symbols

- α, thermal diffusivity;
- μ, viscosity;
- ν, kinematic viscosity;
- ρ, density.

Subscripts

- l, liquid property at T_∞;
- f, liquid property at $T_f = \frac{1}{2}(T_{sat}+T_\infty)$;
- v, vapor property at saturation.

INTRODUCTION

DIRECT contact heat transfer is a mode whereby the participating fluids share a common interface, without the presence of an intervening wall. The attractive features of the direct contact approach are that it obviates the need for conventional heat exchange equipment and provides the possibility of higher heat-transfer coefficients and/or of greater surface area for the transfer process. Examples of applications involving direct contact heat transfer are humidification and spray drying and cooling.

The direct contact mode is often employed in conjunction with a phase change process. For instance, liquid droplets injected into an immiscible liquid will evaporate and become vapor bubbles, provided that the temperature of the receiving liquid is sufficiently high. Similarly, vapor bubbles will condense when introduced into a liquid whose temperature is lower than the saturation temperature of the vapor. The direct contact condensation of steam bubbles in a tank of pressurized water has been suggested as a means of storing thermal energy in a solar-fueled electric power plant [1]. That application was the initiating motivation for the basic research which is reported here.

In the experiments, saturated steam bubbles approximately 3 mm (0.12 in) in diameter were introduced into a quiescent, subcooled water environment. An upward motion was imparted to the bubbles by buoyancy and, owing to heat transfer and condensation at the liquid–vapor interface, the bubbles diminished in size as they ascended. The collapse histories of the bubbles were photographed with a high speed motion picture camera. From a detailed frame by frame analysis of

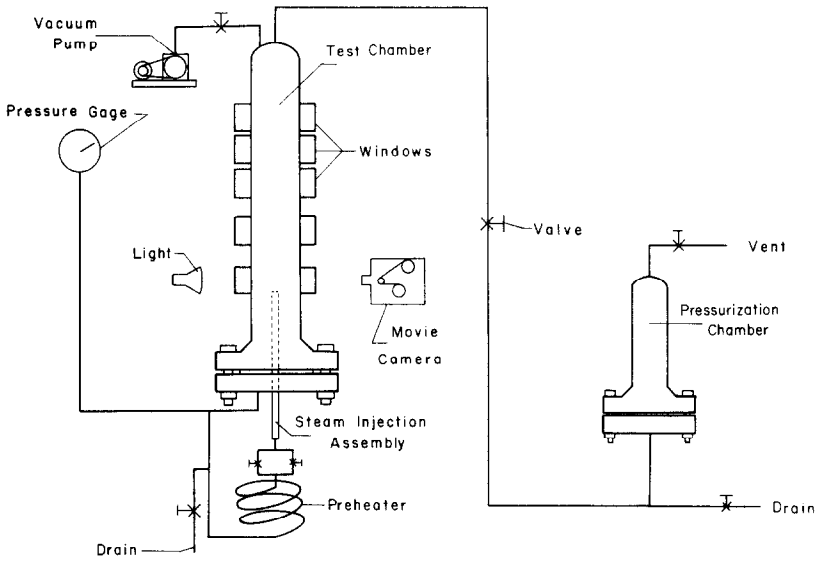

FIG. 1. Schematic diagram of the experimental apparatus.

the photographs, the time variations of the bubble volume, surface area, and position were determined. From these, results were deduced for the time and height for bubble collapse, bubble velocity, average heat transfer coefficient, and instantaneous heat-transfer coefficient. Dimensionless correlations were obtained for various of the aforementioned quantities. The experiments were performed for pressure levels ranging from about 10 to 62 bar (150–900 lb/in^2) and for temperature differences between the saturated steam and subcooled water from 15–100°C.

A review of the literature revealed the fact that prior research on direct contact condensation of steam bubbles in water had been concerned exclusively with operation at atmospheric pressure and, in the main, with relatively small temperature differences. In the experiments of Grassmann and Wyss [2], bubbles were injected into a slightly subcooled environment (< 3°C) at a frequency of about 20 per second. Wittke and Chao [3] investigated the collapse of a single isolated bubble for parametric values of bubble velocity (attained by operating at reduced gravity) for subcooling up to 10°C. The measured collapse histories were in satisfactory agreement with their numerical solution of the governing conservation equations. The Bankoff–Mason experiments [4] dealt with a highly turbulent situation wherein a bubble train (from 200–2500 bubbles per second) was injected into a countercurrent jet of water subcooled to temperature differences up to 70°C.

Sideman and co-workers have made a number of contributions, both analytical and experimental, to the literature on direct contact heat transfer in the presence of a phase change. In general, their experimental work has been directed to two-component immiscible systems, with the exception of pentane/pentane (e.g. [5]), and the steam/water system appears not to have been investigated. The analytical findings of these investigators will be referred to later in the paper.

EXPERIMENTAL APPARATUS

The apparatus that was employed for the acquisition of the data to be reported here is the end result of an evolutionary process in which a succession of modifications were made to cope with the difficult operating conditions of the experiment. Only a general description of the apparatus will be presented in this paper, with additional details being available in [6]. A schematic diagram of the final version of the apparatus is presented in Fig. 1. As pictured there, the main parts of the apparatus are the test chamber situated at the left and the pressurization chamber situated at the right.

The test chamber contains pressurized, subcooled water into which steam bubbles are introduced via the steam injection assembly. The bubbles, which ascend under the action of buoyancy while exchanging heat in the direct contact mode with the liquid, pass through the line of sight of viewing windows. A high speed motion picture camera records the shape of the bubbles as they collapse due to condensation at the liquid–vapor interface.

Under operating conditions, subcooled water is withdrawn from the bottom of the chamber and is ducted to a preheater section where its temperature level is raised. The heated water then passes into the steam injection assembly where it is converted to saturated steam by further heat addition. With proper adjustment of the heat inputs and of the flow control valves situated downstream of the preheater, discrete steam bubbles are produced by an orifice positioned at the exit of the steam injection assembly.

The test chamber is a 91 cm (36 in) high stainless steel pressure vessel with an I.D. of 14.6 cm (5.76 in), designed and fabricated in accordance with ASME standards. It was operated at a maximum pressure of about 62 bar (900 lb/in^2) and a maximum temperature of about 260°C (505°F). Five pairs of diametrically opposite viewing windows were installed at locations

shown in Fig. 1. Only the lowermost pair of windows, which were situated about 13½ cm (5¼ in) above the bottom of the chamber, were employed for photographic data acquisition during the experiments. A 4 kW rod-type immersion heater was positioned in the chamber to facilitate setting the temperature level of the water. To maintain the water temperature, a guard heater was wrapped around the outside surface of the chamber and covered with high temperature insulation. Eight stainless steel sheathed, iron–constantan thermocouples were deployed within the chamber to measure the temperature.

The steam injection assembly consisted of a pair of 91 cm (36 in) long concentric tubes. The 0.16 cm (1/16 in) bore of the inner tube served as the flow passage. The annular gap between the tubes was sealed at both ends and housed a wound wire heating element whose function was to generate steam in the bore. A stainless steel orifice plate, 0.076 cm (0.030 in) thick with a bore diameter of 0.081 cm (0.032 in), capped the top of the injection assembly. To affirm that saturation conditions were actually being attained, a sheathed thermocouple was installed to measure the temperature of the steam at a point 1.6 cm (0.625 in) upstream of the orifice.

The viewing windows merit particular discussion because they presented a difficult problem. Annealed pyrex glass, which might at first appear to be an attractive window material, is attacked by high pressure, high temperature water. Therefore, in commercially available window units, the pyrex is shielded from the water by a mica sheet. Although the pyrex–mica combination is a satisfactory window for general viewing and for back lighting, it does not possess the optical qualities that are requisite for quantitative photography. Warping of the mica, waviness of the pyrex surface, and nonuniform contact at the pyrex–mica interface conspire to produce excessive distortion. In view of these difficulties, quartz windows were substituted for the pyrex, obviating the need for a mica buffer. Furthermore, unlike annealed pyrex, quartz can be polished to provide a distortion-free surface finish. On the other hand, quartz is relatively brittle, and special precautions were required in the gasketing and in the application of torque to the window holders in order to prevent shattering. As finally assembled, each window provided a 2.54 cm (1 in) diameter viewing circle.

The bubbles were photographed with a WF 7 Wollensak Fastex camera. For most of the data runs, the camera was operated at a speed setting of 400 frames per second, using 16 mm Tri-X reversal film. Timing marks were printed on the film at the rate of 120 per second. Back lighting was provided by a 500-W photographic spotlight placed behind the window situated opposite to that through which the bubble was being viewed.

The camera recorded the entire field of view provided by a window. For the data runs, it was positioned at the lowermost viewing window. The steam injection assembly was adjusted so that the top of the orifice plate was just visible at the bottom of this window.

As will be explained in the forthcoming Procedure section, the pressure level in the test chamber was set and maintained with the aid of a pressurization chamber which is pictured schematically at the right in Fig. 1. This chamber, which was designed and fabricated according to pressure vessel codes, is about 32 cm (12½ in) high and 10 cm (4 in) in internal diameter, and is covered with a thick blanket of insulation. Under operating conditions, it was filled with water whose pressure could be varied by heating via two 1.5 kW rod-type immersion heaters. The pressure level in the pressurization chamber was conveyed to the test chamber via a pipeline fitted with a valve to regulate the degree of communication.

EXPERIMENTAL PROCEDURE

The objective of the apparatus design (and of all subsequent modifications) was to obtain a controlled flow of bubbles under conditions where the pressure level and the degree of subcooling could be set at preselected values. Another design objective was to provide means for reducing the amount of soluble non-condensable air in the water to a level where it would not affect the results. The problem of the presence of air in the condensation of steam has been frequently noted in both research and applied publications. In the present research, exhaustive efforts, extending over a period of from 24–48 h, were made to reduce the residual air prior to each set of data runs. Once these preparations were completed, the system temperature and pressure parameters were set and the data acquisition initiated.

The procedure employed for removing the residual air will now be outlined (details can be found in [6]). The test chamber was filled with water and a connection was made between the top of the chamber and a vacuum pump (see Fig. 1). With the pump in operation, a low pressure was maintained in the space above the water, so that boiling occurred at the free surface. To promote a stirring action in the water, power was applied to the preheater and to the steam injection assembly, and the resulting boiling produced a vigorous flow of bubbles from the assembly into the chamber. The steam–air bubbles travelled upward through the chamber under the action of buoyancy. Whereas the steam condensed, the air bubbles reached the free surface and were removed from the system by the vacuum pump.

This procedure was continued until air bubbles were no longer observed travelling upward through the chamber, which occurred after 24–48 h. Only a small amount of water was lost because the temperature of the water in the chamber did not differ appreciably from room temperature (and the vapor pressure was, therefore, relatively low).

Then, to achieve a further reduction in air content, the water temperature was raised by energizing the immersion heater in the test chamber. An increase in temperature reduces the solubility and, therefore, results in the liberation of air. However, the higher temperature also increases the vapor pressure and gives

rise to a larger loss of water from the system. Consequently, pumping was discontinued when the water temperature reached 75°C and, at this point, the air removal operations were terminated.

The immersion heater continued to be energized until the water temperature corresponding to the desired degree of subcooling was attained, at which time the power was turned off and the temperature was maintained by the guard heater on the outside of the test chamber. In the meanwhile, the heaters in the pressurization chamber had been energized. By suitable adjustment of these heaters, the pressure level in the test chamber was set at the desired value.

The adjustment of the power input to the steam injection assembly in conjunction with the adjustment of the valves upstream of the assembly provided a degree of control of the frequency of bubble production. The initial objective was to obtain bubbles at the rate of about one per second. It was found, however, that bubble production was erratic when settings were made in an attempt to obtain such low frequencies. The lowest frequency at which a regular production of bubbles could be obtained was about five per second, and this was the condition for which most of the data were taken.

At each operating condition characterized by a pressure level and a steam–water temperature difference, bubble collapse histories were photographed for a period of 6–10 s. For all data runs, the temperature stratification in the test chamber was less than 3°C per meter (note that the bubbles were viewed over a path length of 0.025 m).

Data were taken at six (nominal) pressure levels—10.3, 20.7, 31.0, 41.4, 51.7 and 62.1 bar, which respectively correspond to 150, 300, 450, 600, 750 and 900 lb/in^2. At each pressure level, data runs were made at (nominal) values of $(T_{sat}-T_\infty)$ of 15, 20, 25, 30, 40, 60, 80 and 100°C.

DATA REDUCTION

The basic information needed for the evaluation of the bubble collapse and heat transfer characteristics is the timewise variation of the bubble volume and surface area. This information was obtained from a detailed frame by frame analysis of the bubble photographs. The method of analysis employed here differs in a basic way from methods used in prior studies of bubble motion and collapse. Previous workers have assumed that the bubble could be regarded as a body of revolution of simple shape, typically an ellipsoid. Consequently, only two dimensions of the observed bubble cross section were measured for the determination of the major and minor axes. However, as has been well documented in the literature and confirmed by the present experiments, bubble shapes may be highly irregular and, therefore, do not conform to the aforementioned data reduction procedure.

In the present approach, a digitizer was employed to record the coordinates of the bubble perimeter (typically at between 40 and 100 points) from highly enlarged projections of the successive frames of film. From the digitized data, the coordinates of the center of mass were evaluated by numerical integration. Then, the orientation of the principle axes was determined so that the product of inertia with respect to these axes is zero. The principle axis closest to the vertical was assumed to be the axis of rotation of the bubble. The volume and surface area were respectively calculated by rotating the bubble cross section and its perimeter about this axis.

The time coordinate associated with each frame was taken from the timing marks on the film, with $t = 0$ corresponding to the frame immediately preceding that in which complete detachment of the bubble from the orifice was first observed.

The next step was to smooth and generalize the data by fitting curves to the discrete volume vs time and area vs time information generated from the digitizing procedure. A number of candidate functional forms were considered. In choosing among these, it appeared reasonable to work with those functional forms which had been derived in the analysis of bubble condensation [7]. It was also found that these functional forms fit the data better than the others that were examined.

In [7], Moalem and Sideman analyzed direct contact condensation both in the absence and presence of noncondensable gases. For the case without noncondensables, their volume vs time relationship can be phrased in the form

$$(V/V_{max})^{1/2} = C_1 + C_2 Fo_m \tag{1}$$

where V is the volume at time t and Fo_m is a dimensionless time (i.e. the Fourier number) based on an equivalent spherical radius $(3V_{max}/4\pi)^{1/3}$. The quantity V_{max} will be discussed shortly. The Moalem–Sideman equation for direct contact condensation in the presence of a noncondensable is quite complex and is not convenient for curve fitting. For cases characterized by small amounts of noncondensable, the equation can be reduced to [6]

$$Fo_m = C_3 + C_4(V/V_{max})^{1/2} + C_5(V/V_{max})^{-1/2}. \tag{2}$$

From visual observations of bubble collapse and from graphs of bubble volume vs time, it appeared that small amounts of residual air were present in some cases, in spite of the extensive efforts that had been made to purge the air from the system. Therefore, equation (2) was used in fitting the data but, for comparison purposes, curve fits were also made using equation (1).

The procedure by which the foregoing equations were employed to fit the data will now be briefly outlined (see [6] for additional details). For a given set of operating conditions defined by pressure level and degree of subcooling, three bubbles were selected for processing from among those on the film strip. For the selection, consideration was given to those bubbles that were most nearly spherical at detachment; also, bubbles having frequencies much greater than five per second were excluded. Since it was a matter of chance as to whether or not the camera would photograph a bubble

at the precise moment of detachment, the observed bubble volume at $t = 0$ is not necessarily its maximum volume. For each of the selected bubbles, the maximum observed volume V_{max} was identified. Then, the V/V_{max} vs Fo_m data for the three bubbles were brought together, and this total population of data was fit, via least squares, with equation (1) and with equation (2). Data characterized by $V/V_{max} < 0.1$ were omitted from the fitting procedure because of the assumptions used in deriving equation (2).

The data for the bubble surface area A were processed in a manner analogous to that employed for the volume [6], using equations similar in form to (1) and (2). The bubble position vs time data were very nearly linear, so that a straight line functional form was employed.

Once the curve fitting had been completed, various quantities of engineering interest were determined. One of these is t^*, the time required for complete condensation of the bubble (i.e. the time at which $V = 0$). The t^* results, deduced from equations (1) and (2) as described in [6], were recast in dimensionless form in terms of Fo^* $(=\alpha_f t^*/r_i^2)$, which will be termed the Fourier number at collapse. The initial bubble radius r_i appearing in Fo^* and in subsequent groups was evaluated as

$$r_i = d_i/2 = [(3V_{max}/4\pi)(V/V_{max})_{t=0}]^{1/3} \quad (3)$$

where $(V/V_{max})_{t=0}$ is obtained from the curve fits, equations (1) and (2), at $t = 0$.

The height to collapse H^* was defined as the distance of the bubble above the orifice plate at the time of collapse. Results for H^* were evaluated by substituting t^* values into the aforementioned linear relationship between bubble position and time and then forming the dimensionless ratio H^*/d_i. Mean velocities v determined from the slope of the position–time curve were represented in terms of the Peclet number $Pe = RePr$.

An average heat-transfer coefficient h^* characterizing the entire condensation process was evaluated from the definition

$$h^* = \frac{(\rho_v V_i h_{fg})/t^*}{(\frac{1}{2}A_i)(T_{sat} - T_\infty)}. \quad (4)$$

Since $\rho_v V_i h_{fg}$ is the amount of energy liberated during the condensation of the bubble, the numerator is the average rate of heat transfer. In the denominator, $\frac{1}{2}A_i$ is taken as the characteristic surface area, and $(T_{sat} - T_\infty)$ is the thermal driving force. The curve fits for V and A were also employed to evaluate an instantaneous heat-transfer coefficient

$$h = \frac{\rho_v(dV/dt)h_{fg}}{A(T_{sat} - T_\infty)} \quad (5)$$

the results for which were ratioed with h^* to achieve a dimensionless representation.

Correlation of the results was sought by examining the quality of the representations obtained by employing various combinations of dimensionless groups. It was found that the best correlations (i.e. lowest standard deviations) were obtained when the Jakob and Rayleigh numbers were employed as correlating parameters. As used here, these groups are defined as

$$Ja = \rho_f c_{pf}(T_{sat} - T_\infty)/\rho_v h_{fg},$$
$$Ra = [g(\rho_l - \rho_v)d_i^3/\rho_f \nu_f^2]Pr_f \quad (6)$$

where the subscript f denotes liquid properties evaluated at $T_f = \frac{1}{2}(T_{sat} + T_\infty)$, and ρ_l is the liquid density at T_∞. All property values for both steam and water were taken from [8].

RESULTS AND DISCUSSION

Bubble collapse patterns

The patterns of bubble collapse will be presented via photographs selected from the motion picture film strips and via graphs of instantaneous bubble volume vs time. Owing to space limitations, only a representative sample of the results can be presented here (a fuller presentation is made in [6]).

Figures 2 and 3 display typical photographic histories which illustrate the observed similarities and differences in the patterns of bubble collapse. In the photographs, the black horizontal region near the bottom is the orifice plate, whereas the black circular region near the top is the upper part of the window assembly. The distance between the orifice plate and the top of the window is about 2 cm. The elapsed time between successive photographs is noted in each figure.

During the initial stages of their lifetimes, all bubbles appear to experience a similar geometric collapse history. At the point of incipient detachment, the bubble is pear shaped, with an umbilical-like attachment to the orifice plate. Upon detachment, the bubble becomes spherical and rises under the action of buoyancy. As it rises, the bottom of the bubble begins to flatten until a hemispherical shape is attained. Then, the top of the bubble begins to flatten, and the bubble becomes a highly eccentric ellipsoid. Long-lived bubbles, such as that of Fig. 2, return to a spherical shape. Studies of the film strips for numerous long-lived bubbles indicated that they collapse as spheres. On the other hand, short-lived bubbles, as in Fig. 3, collapse as ellipsoids. These trends are similar to those observed by Bankoff and Mason [4] under very different experimental conditions.

The results of Figs. 2 and 3 suggest that the time for bubble collapse is significantly increased with increasing pressure. This finding is verified by the results of the other data runs. In addition, it was found that, as expected, the collapse time decreased as the degree of subcooling increased at any fixed pressure level.

Careful observation of all the available photographic information indicates that the aforementioned hemispherical and ellipsoidal bubble shapes occur at times that are more or less common for all bubbles. Typically, these shapes are respectively attained within 0.01 and 0.02 s after detachment. Thus, these characteristic shapes occur at a much smaller fraction of the overall

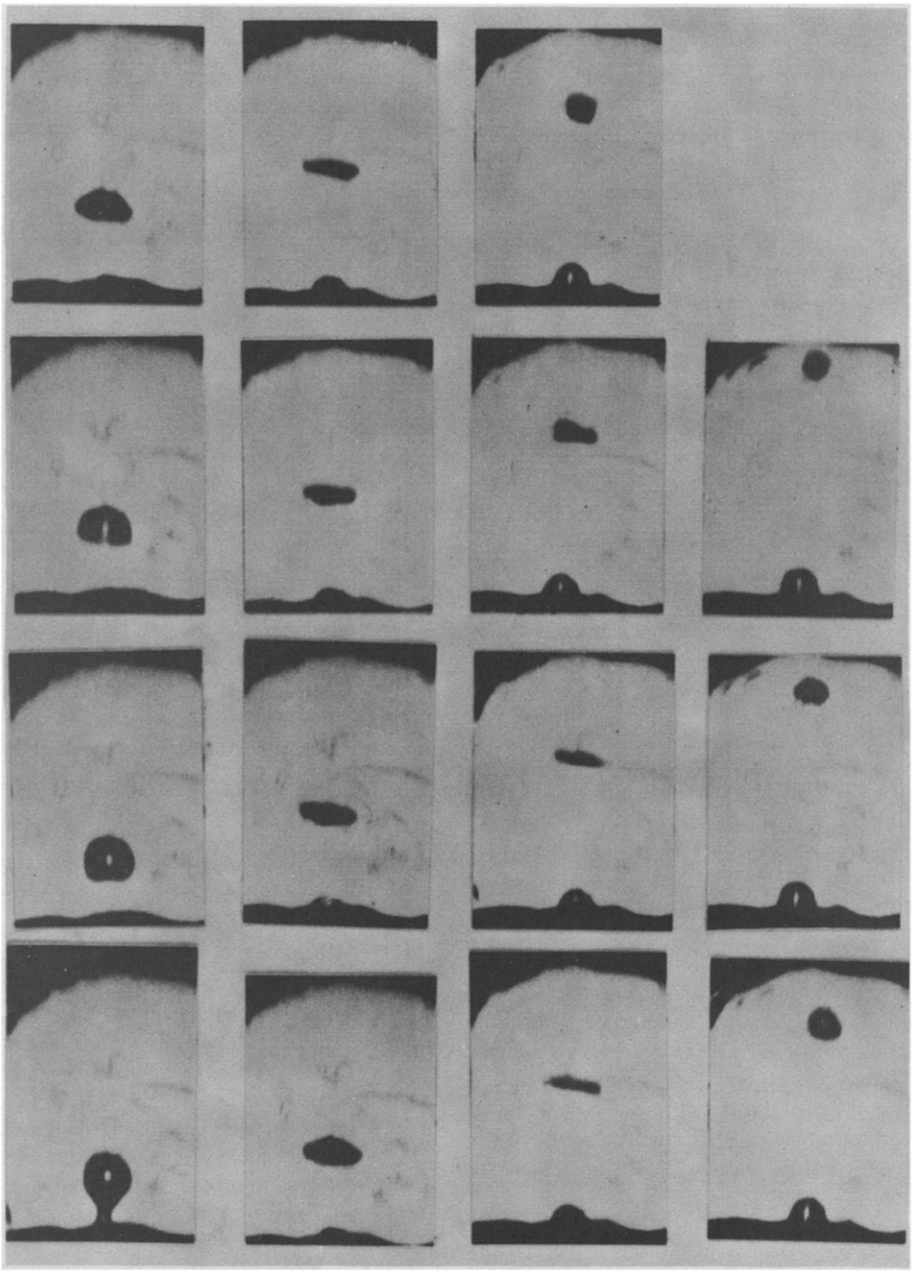

FIG. 2. Bubble collapse history at 41.4 bar and $\Delta T = 31°C$. Elapsed time between successive pictures is 0.0038 s.

lifetime of long-lived bubbles than of short-lived bubbles, thereby suggesting that the former have more compliant interfaces. This is consistent with the fact that the long-lived bubbles are generally associated with higher temperatures which, in turn, correspond to lower surface tension and lower liquid viscosity.

Many of the findings of the preceding paragraphs are further illuminated by the volume vs time results that are presented in Figs. 4 and 5 in the form of V/V_{max} vs Fo_m. These figures respectively correspond to pressure levels of 10.3 and 62.1 bar (150 and 900 lb/in^2). In each figure, data are plotted for a high and a moderate degree of subcooling. The three bubbles that were analyzed at each operating condition are distinguished by different data symbols. Also shown in the figure are curves representing the least squares fits in terms of the functional forms (1) and (2).

Examination of these figures confirms the foregoing observation that the time to collapse is increased at higher pressure levels and at lower degrees of subcooling. From an examination of all the available data, it was noted that as ΔT varied from 100 to 20°C, the time to collapse increased by a factor of about four. In addition, over the range of pressures from 10.3 to 62.1 bar (150 to 900 lb/in^2), the collapse time increased by approximately a factor of three.

From a comparison of Figs. 4 and 5, it is seen that there is greater data scatter at higher pressures. This

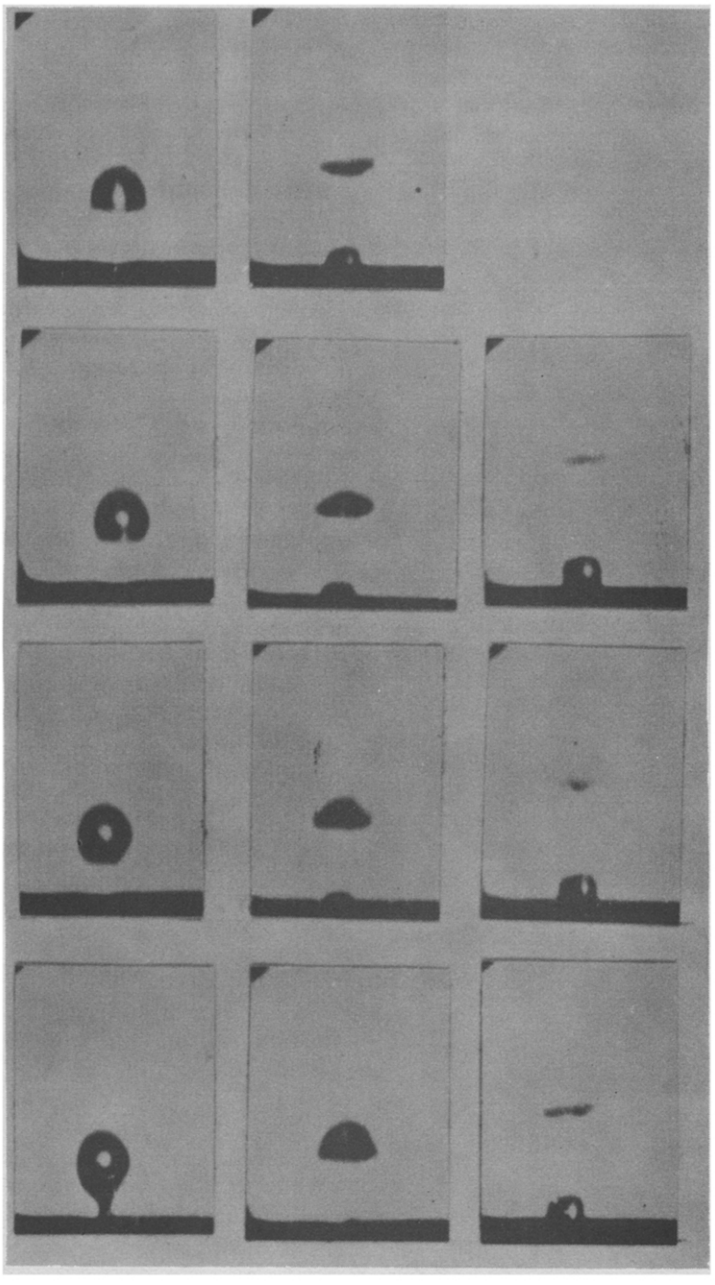

FIG. 3. Bubble collapse history at 10.3 bar and $\Delta T = 30°C$. Elapsed time between successive pictures is 0.0021 s.

scatter is probably the result of oscillations at the bubble interface. As noted earlier, the interface is more compliant at higher pressures owing to the decrease of surface tension and liquid viscosity with temperature and is, therefore, more susceptible to oscillations.

In general, the two-term fit (dashed line) has a shallower shape than does the three-term fit (solid line). Subjectively, it appears that the data are equally well represented by the two fits, and this was corroborated by a comparison of the standard deviations. The fact that the fitted curves do not necessarily intersect the ordinate axis at $V/V_{max} = 1$ is consistent with the meaning of V_{max} as discussed earlier.

Another characteristic of the bubble collapse history is the position of the bubble as a function of time. In this investigation, the instantaneous position of the bubble was evaluated as the vertical height H between its center of mass and the top of the orifice plate. A representative plot (at an intermediate pressure level) showing position vs time data is given in Fig. 6. The straight line passing through the data is a least squares fit. It may be noted that $H/r_{max} > 1(\sim 2)$ at $Fo_m = 0$. This reflects the presence of the umbilical connection between the bubble and the orifice plate at the time of detachment.

In general, a straight line was found to be a good representation of the data for all of the operating conditions of the experiments. This is indicative of a

constant rise velocity. A similar characteristic was observed by Moalem and Sideman [7] for bubbles with diameters exceeding 2 mm, but for experimental conditions that differed appreciably from that of the present investigation. The seemingly broad applicability of this finding is worthy of note.

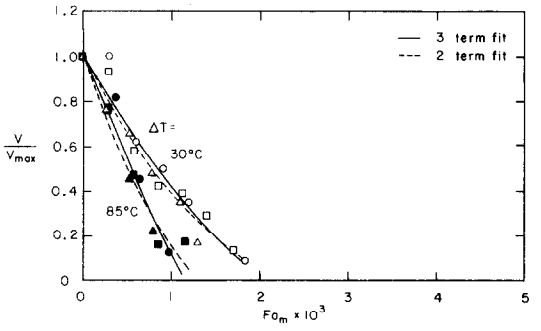

FIG. 4. Variation of bubble volume with time at 10.3 bar.

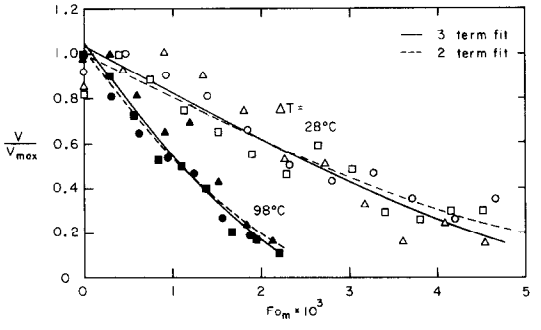

FIG. 5. Variation of bubble volume with time at 62.1 bar.

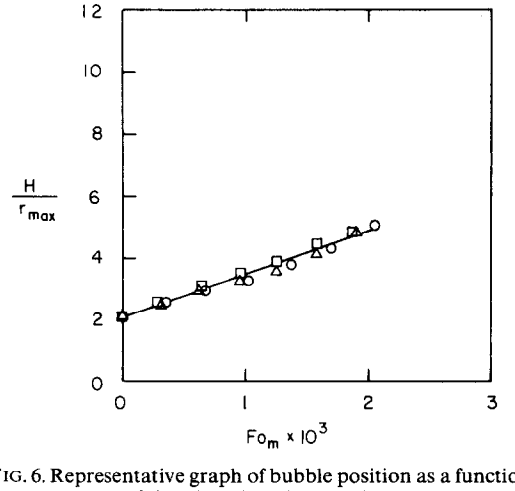

FIG. 6. Representative graph of bubble position as a function of time (41.4 bar, $\Delta T = 98°C$).

For all of the operating conditions, the velocities deduced from the slopes of the position–time straight lines were confined to the relatively narrow range from 16 to 22 cm/s. When these velocity results were placed in dimensionless form in terms of the Peclet number, it was found that essentially all the data were in the range $Pe = 2000$–3000 (see Fig. 5-28 of [6] for details).

Time and height to collapse

The two least squares fits of the volume vs time data, equations (1) and (2), were both employed in deducing values of the time t^* at bubble collapse. Generally, the times obtained from the two fits agreed to within 15% (Fig. 5-26 of [6]). The t^* results to be presented here are based on equation (2).

A tabulation of t^* values, available elsewhere [6], will not be repeated here, but a few representative results will be presented in order to confirm the trends that were mentioned earlier. At a pressure level of 10.3 bar (150 lb/in^2), t^* ranged from 0.08 to 0.016 s as ΔT was varied from 20 to 100°C. The corresponding t^* range at 62.1 bar (900 lb/in^2) was from 0.20 to 0.054 s. The decrease of t^* with increasing temperature difference is consistent with the higher rates of heat transfer per unit area that accompany an increase in the thermal driving force. The effect of pressure is made plausible by noting that the latent heat per unit volume increases significantly with pressure, necessitating a longer bubble lifetime for the transfer of the heat liberated by condensation.

The t^* results have been recast in dimensionless form in terms of the Fourier number $Fo^* = \alpha_f t^*/r_i^2$ and correlated in terms of the Jakob and Rayleigh numbers defined in equation (6). The correlating equation is

$$Fo^* = 55.5/Ja^{3/4}Ra^{1/2}. \tag{7}$$

Eighty-five per cent of the data fall within ±25% of the line represented by equation (7). The data and the correlating line are shown in Fig. 7. It can be seen that the deployment of the data follows a pattern in which three (or two) identical data symbols fall close together along a horizontal line. These clustered data correspond to the three different bubbles for a given operating condition. Owing to the data reduction procedure, they have the same value of Fo^*, but their Rayleigh numbers differ slightly because of small differences in initial diameter d_i.

With respect to the height to collapse H^*, the near constancy of the bubble rise velocity gives

$$H^* \sim C_6 t^* + C_7. \tag{8}$$

Therefore, the trends of H^* with respect to pressure level and to temperature difference are identical to those already identified for t^*. The dimensionless H^* results have been correlated in the form

$$H^*/d_i = 768/Ja^{3/5}Ra^{1/4} \tag{9}$$

and are plotted in Fig. 8. The collapse heights are seen to range from about 2 to 15 times the initial diameter of the bubbles depending on the operating conditions.

Heat-transfer coefficients

Average heat-transfer coefficients h^* were evaluated in accordance with equation (4) and are available in Table 5-1 of [6]. The general level of h^* is 10^4 W/m$^2 \cdot$ °C (1750 Btu/h $\cdot$ ft$^2 \cdot$ °F). Essentially all of the h^* values for all the operating conditions investigated fall within ± 50% of the aforementioned. This is a remarkable

result considering that the pressure level ranged from about 10 to 60 bar and the ΔT varied from 100 to 15°C. It would appear that for design purposes, an h^* value of 10^4 W/m$^2 \cdot$°C can be used with a reasonable level of confidence. The tabulated results show an overall tendency for h^* to increase with pressure. There does not appear to be a clear trend of h^* with ΔT.

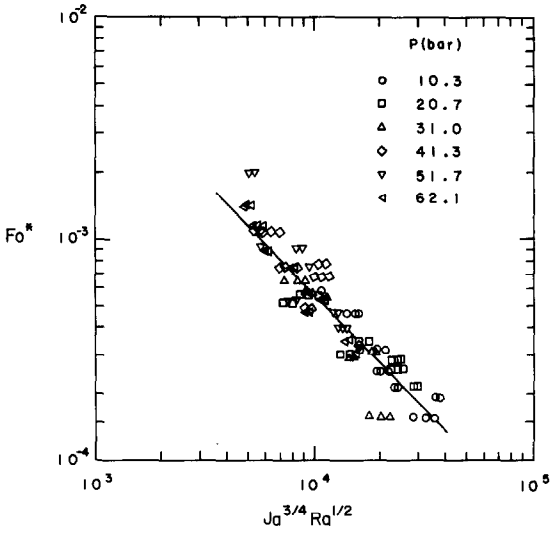

FIG. 7. Dimensionless correlation of the time at bubble collapse.

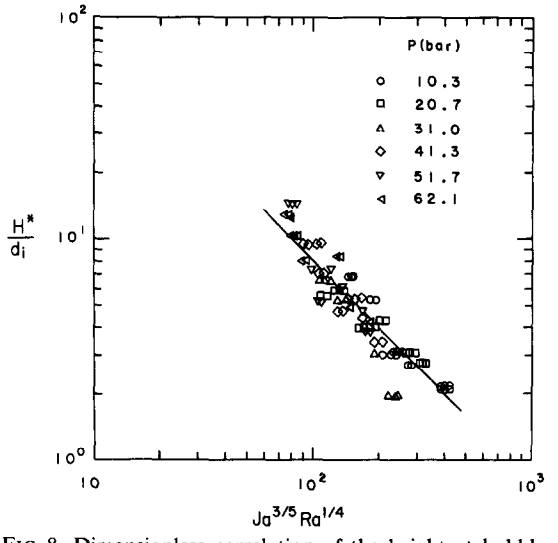

FIG. 8. Dimensionless correlation of the height at bubble collapse.

The present values of h^* are in good agreement with those computed (by the present authors) from the data of Wittke and Chao [3], but are substantially lower than those measured by Bankoff and Mason [4] in a highly turbulent jet impingement configuration. They are also somewhat lower than those of Grassmann and Wyss [2] who employed a bubble injection arrangement less constraining with respect to liquid entrainment than that used here. As noted earlier, all of the aforementioned investigators dealt with the steam/water system at atmospheric pressure.

The h^* values were recast as Nusselt numbers in the form $h^* d_i/k_f$. In addition, by employing the equation $Nu = 0.37Re^{0.6}$ [9], Nusselt numbers were evaluated for a *solid* sphere having a diameter equal to d_i and a velocity equal to that of the bubble. A comparison ([6], Table 5-4) shows that the bubble Nusselt numbers are generally within $\pm 50\%$ of those for the solid sphere.

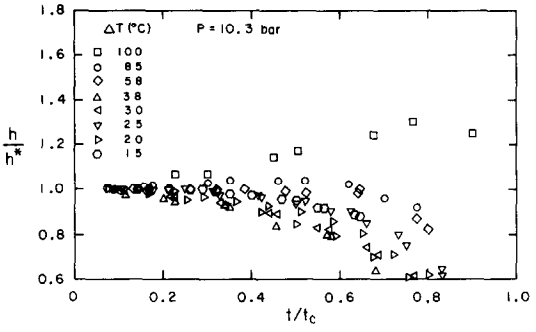

FIG. 9. Instantaneous heat-transfer coefficients at 10.3 bar.

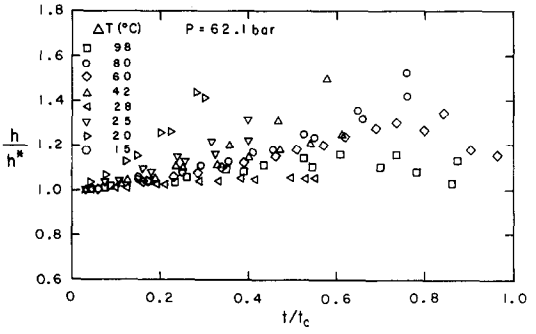

FIG. 10. Instantaneous heat-transfer coefficients at 62.1 bar.

This outcome is quite remarkable in view of the differences between a solid sphere and a condensing vapor bubble. It suggests that the aforementioned solid-sphere Nusselt number equation can be used, in first approximation, to estimate h^*.

Instantaneous heat-transfer coefficients evaluated from equation (5) are presented in detail in Figs. 5-29–5-40 of [6] and illustratively in Figs. 9 and 10 of the present paper. The quantities dV/dt and A appearing in equation (5) were based on three-term least squares fits of the bubble volume and surface area histories [e.g. equation (2)]. Figures 9 and 10 correspond respectively to the lowest and highest pressure levels of the experiments.

The figures indicate an overall trend with pressure wherein h tends to decrease with time at the lower pressures and to increase with time at the higher pressures. There appears to be no consistent trend with ΔT. From a study of Figs. 9 and 10 as well as of the other figures available in [6], it is seen that essentially all of the h/h^* values in the range $0 < t/t^* < 0.8$ lie between 0.6 and 1.5. Thus, h^* serves as a reasonably good measure of the instantaneous values of h.

CONCLUDING REMARKS

The experiments reported here are, apparently, the first to deal with condensation of steam bubbles at elevated pressures (10.3–62.1 bar). In the experiments, saturated steam bubbles approximately 3 mm in diameter were introduced into a quiescent water environment subcooled by 15–100°C. High-speed motion pictures of the bubble collapse histories were processed on a frame by frame basis by a much more detailed procedure than that used in prior investigations of bubble motion and condensation. The coordinates of the bubble perimeter were recorded in digital form and, with these, the center of mass and the principle axes were deduced. The volume and surface area of each bubble were then determined by respectively rotating the bubble cross section and perimeter. From the instantaneous volumes and surface areas, quantitative information about the bubble collapse history and the heat transfer coefficient was obtained.

The photographs showed that during collapse, the bubble shape proceeded successively from a sphere to a hemisphere to an ellipsoid to a sphere to collapse. Short-lived bubbles collapsed as ellipsoids. The time to collapse and the height to collapse were found to increase with increasing pressure and with decreasing temperature difference. Dimensionless collapse times and heights were correlated with the Jakob and Rayleigh numbers, respectively by equations (7) and (9). The rise velocities of the bubbles were essentially constant, with an overall range of 15–22 cm/s; the corresponding Peclet numbers ranged from 2000 to 3000.

Average heat-transfer coefficients h^* evaluated from equation (4) were on the order of $10^4\,W/m^2 \cdot °C$. For all of the operating conditions of the experiments, the h^* were within $\pm 50\%$ of the aforementioned value, thereby establishing its use as a design quantity. Furthermore, the h^* values were found to be within $\pm 50\%$ of those for a *solid* sphere having a diameter equal to the initial bubble diameter and a velocity equal to that of the bubble. Instantaneous heat-transfer coefficients tended to either increase or decrease with time depending on pressure level, but the departures from h^* were only moderate.

Acknowledgement—This research was performed under the auspices of Grant No. GI-34871, initially from NSF (RANN) and subsequently from ERDA.

REFERENCES

1. E. M. Sparrow, J. W. Ramsey, G. K. Wehner *et al.*, Research applied to solar thermal power systems, Report No. 3, University of Minnesota/Honeywell, Inc., Minneapolis, Minnesota (1974).
2. P. Grassmann and E. Wyss, Bestimmung von Wärme- und Stoffübergangszahlen zwischen Dampfblase und Flüsigkeit, *Chem.-Ingr-Tech.* **34**, 755–759 (1962).
3. D. D. Wittke and B. T. Chao, Collapse of vapor bubbles with translatory motion, *J. Heat Transfer* **89**, 17–24 (1967).
4. S. G. Bankoff and J. P. Mason, Heat transfer from the surface of a steam bubble in a turbulent subcooled liquid stream, *A.I.Ch.E. Jl* **8**, 30–33 (1962).
5. D. Moalem, S. Sideman, A. Orell and G. Hetsroni, Direct contact heat transfer with change of phase: condensation of a bubble train, *Int. J. Heat Mass Transfer* **16**, 2305–2319 (1973).
6. G. G. Brucker, Direct contact heat transfer with change of phase at high pressure in a steam–water system, Ph.D. Thesis, University of Minnesota (1976).
7. D. Moalem and S. Sideman, The effect of motion on bubble collapse, *Int. J. Heat Mass Transfer* **16**, 2321–2329 (1973).
8. E. Schmidt, *Properties of Steam in SI Units*. Springer, New York (1969).
9. W. H. McAdams, *Heat Transmission*, 3rd edn. McGraw-Hill, New York (1954). (Note that the referenced equation applies for $Pr \sim 1$, as is the case for water at high temperature.)

CONDENSATION PAR CONTACT DIRECT DES BULLES DE VAPEUR DANS L'EAU A PRESSION ELEVEE

Résumé—Des expériences sur la condensation par contact direct ont été faites avec des bulles de vapeur introduites dans un environnement d'eau au repos et sous-refroidie. Elles concernent un domaine de pression entre 10,3 et 62,1 bar, un sous-refroidissement entre 15 et 100°C et des diamètres de bulles initiaux de trois millimètres environ. La réduction des données des prises de vues à grande vitesse est basée sur l'analyse image par image dans laquelle les coordonnées du périmètre de la bulle sont enregistrées sous forme digitale et traitées pour donner une information quantitative sur l'histoire de la bulle et sur le coefficient de transfert thermique. Les photographies montrent que les formes successives des bulles durant leur histoire vont de la sphère à un hémisphère, à un ellipsoïde, à une sphère puis au collapsus; les bulles à existence courte collapsent en ellipsoïde. Le temps de disparition et la hauteur de collapsus croissent quand la pression augmente et quand décroît la différence de température. Les vitesses d'ascention des bulles sont essentiellement constantes avec un domaine global de 15–22 cm/s. Les coefficients moyens de transfert thermique sont de l'ordre de $10^4\,W/m^2\,K$ avec seulement des variations modestes en fonction du niveau de pression et de la différence de température. Les coefficients de transfert instantanés ne diffèrent pas sensiblement des coefficients moyens.

DIE KONDENSATION VON DAMPFBLASEN IN DIREKTEM KONTAKT MIT HOCHDRUCKWASSER

Zusammenfassung—Es wurden Versuche zur Untersuchung der Direktkontakt-Kondensation von gesättigten Dampfblasen, die in ruhendes, unterkühltes Wasser eingeleitet werden, durchgeführt. Die Versuche erfolgten bei Drücken von 10,3 bis 62, 1 bar, bei Unterkühlungen von 15–100 K und bei Anfangsblasendurchmessern von etwa 3 mm. Hochgeschwindigkeits-Filmaufnahmen wurden im Einzel-

bildverfahren ausgewertet, wobei die Blasenumfangskoordinaten digital aufgenommen wurden und anschließend zur quantitativen Ermittlung der Blasenzerfallsgeschichte und des Wärmeübergangskoeffizienten verwertet wurden. Die Fotografien zeigten, daß die Blasen während des Zerfalls nacheinander Kugelform, Halbkugelform, Ellipsoidform und noch einmal Kugelform annehmen; kurzlebige Blasen zerfielen schon als Ellipsoide. Die Zerfallszeit und die Höhe, bei welcher der Zerfall eintritt, nahmen mit zunehmendem Druck und abnehmender Temperaturdifferenz zu. Die Aufstiegsgeschwindigkeit der Blasen war im wesentlichen konstant und lag im Bereich von 15–22 cm/s. Die mittleren Wärmeübergangskoeffizienten lagen in der Größenordnung von 10^4 W/m^2 K und variierten nur geringfügig mit dem Druck und der Temperaturdifferenz. Die momentanen Wärmeübergangskoeffizienten wichen nur wenig von den mittleren Wärmeübergangskoeffizienten ab.

ПРЯМАЯ КОНТАКТНАЯ КОНДЕНСАЦИЯ ПУЗЫРЬКОВ ПАРА В ВОДЕ ПРИ ВЫСОКОМ ДАВЛЕНИИ

Аннотация — Проведены экспериментальные исследования прямой контактной конденсации пузырьков насыщенного водяного пара, вводимых в неподвижный недогретый до кипе, ия объем воды. Эксперименты проводились в диапазоне давлений 10,3–62,1 бар (150–900 фунт/кв. дюйм абс.) при недогреве от 15 до 100°С. Начальный диаметр пузырьков составлял около 3 мм. Снимки, полученные высокоскоростной кинокамерой, расшифровывались с помощью покадрового анализа с цифровой записью координат периметра пузырьков, а затем обрабатывались для получения количественной информации о процессе схлопывания пузырьков и значениях коэффициента теплообмена. На снимках зафиксированы последовательные формы, принимаемые пузырьками до разрушения: сферическая — полусферическая — эллипсоидная — сферическая. Пузырьки с непродолжительным временем жизни разрушались в эллипсоидной стадии. Время жизни и высота подъёма пузырька до схлопывания увеличиваются с увеличением давления и ушеньшением разности температур. Скорость подъёма пузырьков была в основном постоянной и равнялась 15–22 см/сек. Коэффициент теплообмена в среднем составлял 10^4 Wm^2-°C (1750 Btu/h-ft^2-°F) и только незначительно изменялся с изменением давления и разности температур. Текущие значения коэффициента теплообмена не отличались значительно от средних значений.